DELAMINATION INITIATION AND PROPAGATION MODELLING WITH AN ENRICHED SHELL ELEMENT FORMULATION

J. Främby[1], M. Fagerström[1], J. Brouzoulis[1]

[1]Division of Material- and Computational Mechanics, Department of Applied Mechanics,
Chalmers University of Technology, Hörsalsvägen 7, SE-412 96 Gothenburg, Sweden
Email: johannes.framby@chalmers.se

Keywords: shells, delamination, XFEM, computational efficiency

Abstract
For achieving good predictability of the deformation of structural composite components in crash simulations, a proper modelling of the delamination process is crucial. However, due to industrial restrictions on the simulation time of crash simulations, detailed modelling of each ply by separate elements through the thickness is not feasible. A potential remedy is to adopt the concept of adaptive shell elements which can be enriched whenever delaminations need to be accounted for. Hence, a structural model of a thinwalled laminate can thereby initially be built up from a single layer of shell elements through the thickness. During loading, the model is then enriched locally in critical areas where delamination is predicted. In this contribution, we show the potential of such an approach, where delamination cracks are adaptively introduced in the analysis based on a stress criterion in terms of the transverse stresses. A specific challenge is that these stresses are predicted with low accuracy in the FE model, whereby a post-processing step is proposed where an improved prediction is reconstructed based on the momentum balance equations. We show the potential of the proposed methodologys ability to capture initiating and propagating delaminations, and can conclude that the proposed methodology appears to be suitable for the simulation of thin-walled structures undergoing substantial delaminations.

1. Introduction

To meet the increasing demands from regulatory bodies on CO_2 emissions from automotive cars, the automotive industry is currently very active in reducing vehicle weight, where one significant step is to increase the amount of Fibre Reinforced Polymers (FRPs) due to their superior specific properties (*e.g.* specific strength and specific energy absorption in axial crushing) compared to conventional metals. However, as concluded in the European Roadmap to Safe Road Transport [1], the numerical finite element (FE) tools for the accurate prediction of the crash response of vehicle structures in FRPs are crucial for structural composites to have a widespread use in future cars.

Traditionally, FE crash simulations are performed using equivalent single-layer shell element models, which are well suited to model the thin-walled metal structures in automotive bodies while at the same time being computationally cost effective compared to continuum solid (3D) element models. However, to achieve good predictability of the deformation of structural composite components in crash simulations, a proper modelling of the delamination process is crucial. At the same time, industrial restrictions on the simulation time of crash simulations implies that detailed modelling of each ply as represented by separate elements through the thickness is not feasible.

Thus, to be able to perform large scale simulations of progressive crash failure in FRPs (*e.g.* to capture

Excerpt from ISBN 978-3-00-053387-7

delamination, driven by high transverse stresses) while maintaining a good level of predictability, better suited types of FE-models need to be adopted. Prerequisites for such models are that they need to be both accurate and computationally efficient – a challenge addressed in this paper. Thereby, we choose to adopt an equivalent single-layer shell model recently proposed by Brouzoulis and Fagerström [2] where delamination failure is described using local extension of the element formulation.

Such element formulations have been proposed by several authors previously. Remmers *et al.*[3] presented a solid-like ESL shell capable of describing an arbitrary delamination using the partition-of-unity modelling concept the eXtended Finite Element Method (XFEM) [4]. This allows for mesh independent representations of arbitrary discontinuities (*e.g.* cracks and delaminations) by introducing kinematic enrichments locally in the vicinity of the propagating crack. A similar approach was recently proposed in Brouzoulis and Fagerström [2] although extended to include an arbitrary number of delaminations. Other partition-of-unity concepts like the phantom node or the floating node approaches have also been used by authors like Ahmed and Sluys [5] and McElroy [6] to model propagating delaminations. A related concept has been proposed by Hosseini *et al.*[7], where a shell element based on the isogeometric analysis concept is extended to model propagating delamination by modifying the knot-vector associated to the thickness interpolation. Regardless of the chosen method, the common idea is that the delamination enrichments can be made locally. However, if the methods are to be computationally efficient they must be used in a methodology which is able to asses when and where to insert the enrichments.

An emerging challenge is therefore the fact that through-the-thickness predicted transverse (out-of-plane) stress components are predicted with low accuracy when using traditional shell element formulations [8]. This issue was addressed in a previous work by the authors [9], where it was concluded that the traditional post-processing recovery method for improving the prediction of the transverse stresses provides acceptable results for mechanical loading, as also concluded in the reviews by Carrera [10] and Noor and Malik [11]. In this work we further develop this recovery method and use it to locate critical areas where the adopted shell formulation can be locally enriched, such that the kinematics of delamination can be captured even using an equivalent single-layer model.

2. Shell formulation for multiple delaminations

To set the stage, we start by presenting the adopted kinematic shell framework proposed by Brouzoulis and Fagerström [2]. The framework consists of three interrelated domains; the inertial Cartesian domain $\mathcal{B}_C$, the undeformed (reference) domain $\mathcal{B}_0$ and the deformed domain $\mathcal{B}$ with pertinent mappings, cf. Figure 1.

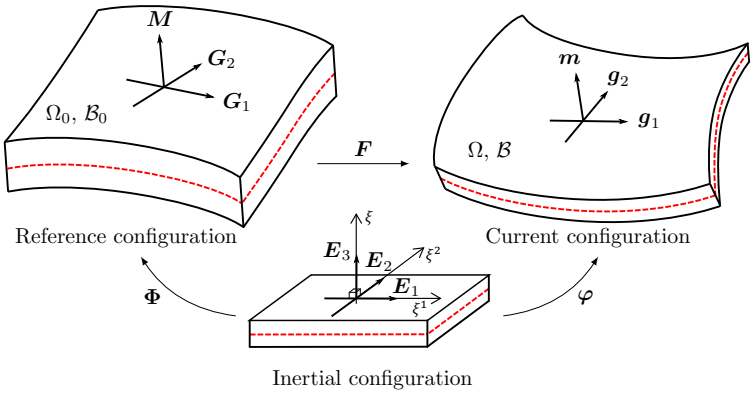

Figure 1. Mappings of shell model defining undeformed and deformed shell domains relative to the inertial Cartesian domain.

Excerpt from ISBN 978-3-00-053387-7

2.1. Initial shell geometry

Following Brouzoulis and Fagerström [2], we have that the reference domain $\mathcal{B}_0$ of the shell is considered parametrised in terms of convected (co-variant) coordinates $\boldsymbol{\xi} = (\xi^1, \xi^2, \xi^3 = \xi)$. This means that a point $\boldsymbol{\xi}$ in the inertial domain is mapped to a corresponding point $\boldsymbol{X}$ in the undeformed domain via the mapping

$$\boldsymbol{X} = \boldsymbol{\Phi}(\boldsymbol{\xi}). \tag{1}$$

In a similar fashion, we have that a point on the mid-surface $\boldsymbol{\xi}_0 = (\xi^1, \xi^2)$ in the inertial domain is mapped to a corresponding mid-surface point $\bar{\boldsymbol{X}}$ in the undeformed domain via

$$\bar{\boldsymbol{X}} = \bar{\boldsymbol{\Phi}}(\boldsymbol{\xi}_0). \tag{2}$$

Associated with the mapping $\boldsymbol{\Phi}$, we also have the co-variant base vectors $\boldsymbol{G}_i$ in the undeformed domain as

$$\boldsymbol{G}_i = \boldsymbol{\Phi}_{,i}, \tag{3}$$

where $\bullet_{,i}$ denotes the partial derivative of $\bullet$ with respect to ξ^i, $i = 1, 2, 3$.

2.2. Deformed shell geometry with multiple delaminations

Similarly to the geometry mapping described above, we also have that the deformed geometry is described by the deformation map $\boldsymbol{\varphi}(\boldsymbol{\xi}) \in \mathcal{B}$ from the inertial Cartesian frame. This means that the deformed position $\boldsymbol{x}$ of a material point $\boldsymbol{X}$ is generally given by

$$\boldsymbol{x} = \boldsymbol{\varphi}(\boldsymbol{\xi}) \tag{4}$$

with the pertinent co-variant base vectors in the deformed domain defined as

$$\boldsymbol{g}_i = \boldsymbol{\varphi}_{,i}. \tag{5}$$

To describe multiple delaminations within one and the same shell element, the above defined spatial deformation map $\boldsymbol{\varphi}$ needs to be extended to allow for displacement discontinuities across delamination interfaces. This is achieved by locally enriching the displacement approximation of the shell in the vicinity of interlaminar cracks in line with the XFEM. Thus, the deformation map of the deformed domain is subdivided into one continuous and one discontinuous part as

$$\boldsymbol{\varphi}(\boldsymbol{\xi}) = \boldsymbol{\varphi}^{\mathrm{c}}(\boldsymbol{\xi}) + \boldsymbol{\varphi}^{\mathrm{d}}(\boldsymbol{\xi}), \tag{6}$$

where the continuous part $\boldsymbol{\varphi}^{\mathrm{c}}$ takes on the form

$$\boldsymbol{\varphi}^{\mathrm{c}}(\boldsymbol{\xi}) = \bar{\boldsymbol{\varphi}}^{\mathrm{c}}(\boldsymbol{\xi}_0) + \xi \boldsymbol{m}^{\mathrm{c}}(\boldsymbol{\xi}_0) + \frac{1}{2}\xi^2 \gamma^{\mathrm{c}}(\boldsymbol{\xi}_0)\boldsymbol{m}(\boldsymbol{\xi}_0) \tag{7}$$

in terms of the deformed mid-surface placement $\bar{\boldsymbol{\varphi}}^{\mathrm{c}}$, the extensible director field $\boldsymbol{m}^{\mathrm{c}}$ and an additional scalar thickness strain γ^{c} (leading to seven degrees of freedom per node for the continuous deformation).

As for the discontinuous part $\boldsymbol{\varphi}^{\mathrm{d}}$, it is constructed as a sum of enrichments (one for each delamination) as

$$\boldsymbol{\varphi}^{\mathrm{d}} = \sum_{k=1}^{\mathrm{N_{del}}} \psi_k \underbrace{\left(\bar{\boldsymbol{\varphi}}^{\mathrm{d}}_k(\boldsymbol{\xi}_0) + \xi \boldsymbol{m}^{\mathrm{d}}_k(\boldsymbol{\xi}_0)\right)}_{\boldsymbol{\varphi}^{\mathrm{d}}_k} \tag{8}$$

where the existing delamination cracks are numbered globally starting from the bottom of the laminate and where ψ_k is a discontinuous enrichment function which is one above delamination crack k and zero elsewhere. To be specific, the enrichment function ψ_k ensures that the particular enrichment $\boldsymbol{\varphi}^{\mathrm{d}}_k$ is introduced only for points inside the delamination zone. However, please note that, since a Heaviside function is used for the enrichment, the continuity requirement $\boldsymbol{\varphi}^{\mathrm{d}}_k = \boldsymbol{0}$ needs to be explicitly enforced along each delamination crack front.

Excerpt from ISBN 978-3-00-053387-7

3. Improved prediction of transverse stresses by stress recovery

To obtain an better prediction of the transverse stresses we propose to use a post-processing stress recovery method where improved values are recovered from the 3D momentum balance equations.

The recovery of the transverse stress variation through the thickness of the shell is made via thickness integration of the 3D momentum balance equations. For zero body forces under quasi-static conditions we can find the transverse stresses (expressed in a co-rotated coordinate system $x_1x_2x_3$) as:

$$\hat{\sigma}^k_{\alpha 3} = -\sum_{n=1}^{k} \int_{x_3^{(n-1)}}^{x_3^{(n)}} (\sigma_{\alpha 1,1} + \sigma_{\alpha 2,2})\, \mathrm{d}x_3 + C_\alpha,\ \hat{\sigma}^k_{33} = \sum_{n=1}^{k} \int_{x_3^{(n-1)}}^{x_3^{(n)}} \int_{x_3^{(n-1)}}^{x_3^{(n)}} (\sigma_{11,11} + \sigma_{22,22} + 2\sigma_{12,12})\, \mathrm{d}x_3 \mathrm{d}x_3 + C_3 x_3 + C_4, \quad (9)$$

where x_3 is the local transverse direction, $x_3^{(n-1)}$ and $x_3^{(n)}$ denote the lower and upper thickness coordinate of ply n, i denotes derivative with respect to coordinate $i = [1, 2]$ and $\hat{\bullet}$ denotes recovered values.

In the case of transverse shear stresses in Eq. (9), the integration constant C_α can be determined from the known value of $\sigma_{\alpha 3}$ at either of the two boundaries at $x_3 = \pm\frac{h}{2}$. In this work we handle this by performing the integral from the bottom of the laminate, starting at the bottom boundary condition, and then calculating the potential integration error at the top surface. The resulting error is then distributed evenly through the thickness, resulting in equal integration errors at the top and bottom surface. Thus, the recovery of the transverse shear stresses does not guarantee to fulfil the boundary shear tractions. For the transverse normal stress $\hat{\sigma}_{33}$ the integration of the second order equation produce two integration constants, which results in automatic fulfilment of the normal traction at the top and bottom surface.

The integrations in Eq. (9) involves the in-plane first and second derivatives of the in-plane stresses, which must be extracted from the FE-solution. To do so we have adopted a technique similar to the *Exact Surface Fitting Method* in [12], where the in-plane stresses in layer k are are approximated using the polynomial fit

$$\sigma^k_{\alpha\beta} = \mathbf{P}(x_1, x_2, x_3)\mathbf{a}_{\alpha\beta} \quad (10)$$

to the integration point stress values. In order to represent quadratic variation of the shear stresses and cubic variation of the normal stress through the thickness of the laminate, we choose the polynomial terms $\mathbf{P}(x_1, x_2, x_3)$ in Eq. (10) to be

$$\mathbf{P}(x_1, x_2, x_3) = [1\ \ x_1\ \ x_2\ \ x_3\ \ x_2x_3\ \ x_1x_3\ \ x_1x_2\ \ x_1^2\ \ x_2^2\ \ x_1^2x_3\ \ x_2^2x_3] \quad (11)$$

with the corresponding unknown coefficients

$$\mathbf{a}_{\alpha\beta} = [a^{(1)}_{\alpha\beta}\ \ a^{(2)}_{\alpha\beta}\ \ a^{(3)}_{\alpha\beta}\ \ a^{(4)}_{\alpha\beta}\ \ a^{(5)}_{\alpha\beta}\ \ a^{(6)}_{\alpha\beta}\ \ a^{(7)}_{\alpha\beta}\ \ a^{(8)}_{\alpha\beta}\ \ a^{(9)}_{\alpha\beta}\ \ a^{(10)}_{\alpha\beta}\ \ a^{(11)}_{\alpha\beta}]^T. \quad (12)$$

When the polynomial coefficients are determined, analytical expressions of Eq. (9) can be created by taking the derivative and and subsequent integral of the stress polynomial in Eq. (10):

$$\hat{\sigma}^k_{\alpha 3} = -\mathbf{P}_{\int_3,1}\, \mathbf{a}_{\alpha 1} - \mathbf{P}_{\int_3,2}\, \mathbf{a}_{\alpha 2} + C_\alpha, \quad (13)$$

$$\hat{\sigma}^k_{33} = \mathbf{P}_{\iint_3,11}\, \mathbf{a}_{11} + \mathbf{P}_{\iint_3,22}\, \mathbf{a}_{22} + 2\mathbf{P}_{\iint_3,12}\, \mathbf{a}_{12} + C_3 x_3 + C_4. \quad (14)$$

where

$$\mathbf{P}_{\int_3,1} = \int_{x_3} \mathbf{P}_{,1}\, \mathrm{d}x_3,\ \mathbf{P}_{\int_3,2} = \int_{x_3} \mathbf{P}_{,2}\, \mathrm{d}x_3,$$
$$\mathbf{P}_{\iint_3,11} = \iint_{x_3} \mathbf{P}_{,11}\, \mathrm{d}x_3\mathrm{d}x_3,\ \mathbf{P}_{\iint_3,22} = \iint_{x_3} \mathbf{P}_{,22}\, \mathrm{d}x_3\mathrm{d}x_3,\ \mathbf{P}_{\iint_3,12} = \iint_{x_3} \mathbf{P}_{,12}\, \mathrm{d}x_3\mathrm{d}x_3 \quad (15)$$

Excerpt from ISBN 978-3-00-053387-7

Please note that with the chosen shell kinematics, the in-plane stress components themselves are predicted with acceptable accuracy. However, as in the case of any C^0-continuous finite element, the stresses from the FE solution are not continuous over element boundaries, meaning that the stress gradients cannot be evaluated from single elements without making some simplifying assumption (cf. *e.g.* [13]). Thus, it is not sufficient to construct the stress polynomial individually within each element. We therefore perform the polynomial fit in Eq. (12) to all the ply integration points in an element patch including the neighbouring elements. Please also note that in order to solve for the chosen polynomial $\mathbf{P}(x_1, x_2, x_3)$ in Eq. (12), it is necessary to have at least three integration points in the thickness and in-plane directions.

4. Adaptive enrichment concept for delamination initiation and propagation

As a criterion for delamination initiation, we choose to adopt a criterion similar to that proposed by Ochoa and Engblom [14]. The criterion features a quadratic relation between the tensile transverse normal and the resulting transverse shear stresses (in our case obtained from the stress recovery):

$$f_{\mathrm{I}} = \left(\frac{\langle \hat{\sigma}_{33} \rangle_+}{\sigma_{\mathrm{fn}}} \right)^2 + \frac{\hat{\sigma}_{13}^2 + \hat{\sigma}_{23}^2}{\sigma_{\mathrm{fs}}^2} \geq r_{\mathrm{I}}^2, \quad 0 < r_{\mathrm{I}} \leq 1. \tag{16}$$

where σ_{fn} and σ_{fs} are the interlaminar tensile normal and shear strength respectively and $\langle \bullet \rangle_+$ is the positive Macaulay brackets. Please note that in order to avoid numerical problems at the point of intiation, we propose to enrich new delmination zones at a stress state somewhat lower than the critical state ($r_{\mathrm{I}} < 1$). Furthermore, when the delamination initiation criterion in Eq. (16) is reached at any interface in any element, all nodes (and elements) within a certain radius R_{I} are enriched. The appropriate initiation level r_{I} and appropriate size of the initiation radius R_{I} are addressed in [15].

The active delamination enrichment and associated cohesive law must be able to evolve properly. This implies that the cohesive zone must be large enough such that the kinematics of the crack is captured correctly. This will in our case, where we introduce delamination enrichments adaptively throughout the analysis, affect how large the size of any active enrichment should be. In order to achieve this, we propose a propagation criterion, which expands the enrichment when necessary. This criterion reaches unity whenever softening of the interface has been introduced anywhere in the delamination, *i.e.* if any of the elements associated with the delamination reaches its interlaminar failure strength and damage has begun:

$$f_{\mathrm{P}} = 1 \quad \text{if} \quad d > r_{\mathrm{P}} \text{ in } \Gamma^{\mathrm{del}}, \tag{17}$$

where r_{P} is a small number close to zero and Γ^{del} represents the surface of a delamination. When the propagation criterion in Eq. (17) becomes active in any element in a delamination, the enrichment is expanded to include all nodes a distance R_{P} from the element nodes. The appropriate damage level r_{P} and expansion radius R_{P} of the delamination enrichment is addressed in [15].

5. Numerical examples

In this section, we verify the proposed methodology by two numerical examples, sketched in Figure 2. In Subsection 5.1, we first demonstrate results from the recovery of the transverse stresses. We consider here a situation with applied tractions on the shell surfaces, and show that the recovery method works well. In the next step, we consider propagation of existing delamination cracks in the analysis of a double cantilever beam (DCB) test. For more examples, we refer interested readers to [15].

5.1. Example 1: Recovery of transverse stresses

To verify the stress recovery method presented in Section 3, we study a simply supported beam subjected to prescribed tractions at the top and bottom surfaces. The geometry of the beam is such that the length to

Excerpt from ISBN 978-3-00-053387-7

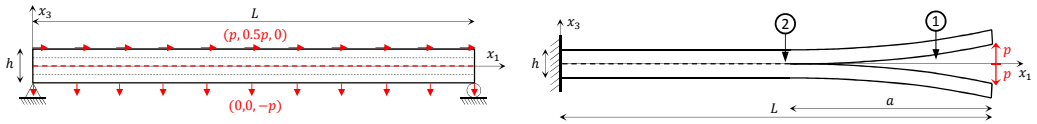

a) b)

Figure 2. a) Geometry of the simply supported beam used in the Example 1. b) Geometry of the DCB test used in the Example 2.

width to thickness ratio is 5:2:1 and the beam has a [90 -45 45 0] layup, cf. Figure 2a. Furthermore, to assess the recovery method, resulting stresses are compared to those from a reference 3D model. The shell model consists of 100 shell elements and the 3D reference model of 43,200 solid elements, respectively. The traction loads consists of a normal tensile component of $p = 1.0$ MPa on the bottom surface and shear components of p and $0.5p$ in the longitudinal and lateral directions on the top surface. To further show the potential of the method to account for interlaminar cracks, we place a delamination zone in the middle interface and add an isotropic elastic cohesive law to transfer the load.

The resulting through-the-thickness variations of the important stress components, at a point $^{L}/_{3}$ from the left support, are plotted in Figure 3. From the results it is clear that the in-plane stresses (σ_{11}) are predicted well using the shell model. It is also shown that the predictions of the transverse stress components (σ_{13} and σ_{33}) are improved using the proposed recovery technique. In addition, the recovery match the boundary conditions of the shear stresses very well, even though these are not explicitly enforced. To conclude, the stress recovery technique shows significant improvements in the prediction of the transverse stresses, even if it is not possible to reach exactly the same level of accuracy as a high-fidelity model. This should however be viewed in the light of computational efficiency where it should be noted that, in this particular example, the solid model requires 31 times as long CPU-time compared to the shell analysis, while additional cost of performing the stress recovery is negligible.

5.2. Example 2: Crack propagation in double cantilever beam test

The double cantilever beam, illustrated in Figure 2b, consists of two plies with fibre directions along the beam and has a length of $L = 200$ mm, it has a height of $h = 3$ mm and a width of $w = 5$ mm. The ply material data are taken as: $E_1 = 126$ GPa, $E_2 = E_3 = 10$ GPa, $G_{12} = G_{13} = G_{23} = 8$ GPa, $\nu_{12} = \nu_{13} = \nu_{23} = 0.29$. The initial delamination crack of length $a = 30$ mm (marked ① in Figure 2b) is modelled using an initial enrichment with zero cohesive traction. Besides this, the first row of elements in the virgin material (location marked ② in Figure 2b) are also enriched, where the cohesive zone model adopted here and for the subsequent crack propagation is the one proposed by Jansson and Larsson [16], with the following interface properties: $\mathcal{G}_{\mathrm{Ic}} = 218$ J/m^2 and $\sigma_{\mathrm{fn}} = 57$ MPa. This way the model has a small region where the damage evolution can be measured such that the propagation criterion in Eq. (17) can be evaluated. The virgin part of the beam is modelled with an in-plane element size of 0.3 mm, while the outer part with initial delamination has a coarser mesh. Finally, in the analysis, the free ends of the beam are subjected to prescribed displacements in the vertical direction with a magnitude p and the resulting reaction forces are calculated.

The influence of different damage levels r_{P} is examined for three cases using a large expansion radius and a load increment of 0.05 mm/step. The results from these analyses are in Figure 4a compared to a reference case, where the entire beam interface is initially enriched. The analytical solution for DCB is indicated as well. The results show that the solution of the fracture process is stable, indicating that the resolution using two elements in the process zone is adequate. We can also conclude that the moment of propagation has converged for damage initiation levels $r_{\mathrm{P}} < 10^{-4}$. If this level is increased the propagation of the enrichment

Excerpt from ISBN 978-3-00-053387-7

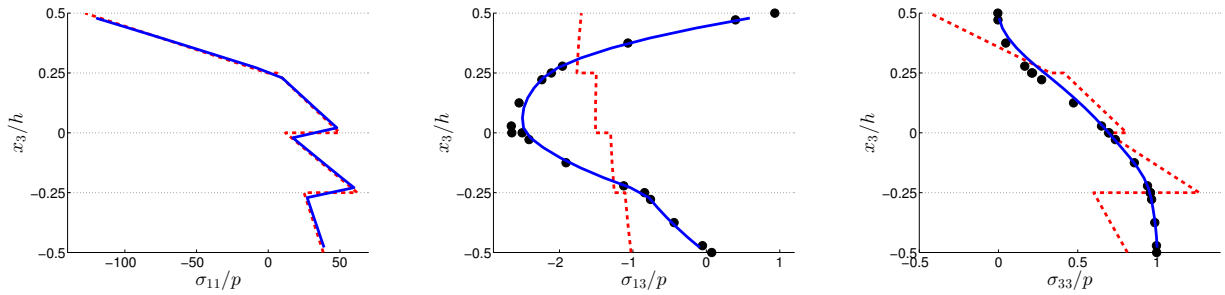

Figure 3. Resulting through-the-thickness stresses in Example 1. Stress components in reference (blue) and shell (red dashed) models together with recovered transverse stresses (•) in analysis of simply supported beam.

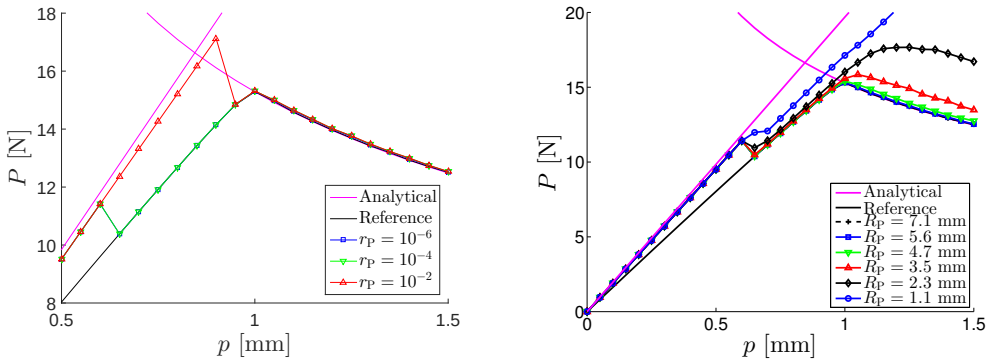

Figure 4. Force-displacement response of DCB test using a) 5.9 mm expansion radius and different damage thresholds and b) a fixed damage threshold and different expansion radii. Please note that in a) only a part of the curve is shown to clarify the differences.

front will be postponed and the force passes the fracture force before the delamination propagates.

Further analyses using $r_P = 10^{-6}$ and different expansion radii R_P are in Figure 4b compared to the reference case and the analytical solution. Here we can observe that having an expansion radius of more than 6 mm leads to results close to the reference solution while shorter distances lead to over-prediction of the maximum force. When the expansion radius is too short the delamination propagation between steps is restricted, which results in an overly stiff response in this displacement controlled test. Based on this, we recommend that the propagation radius should be at least ten times the size of the process zone for mode I. And even for this case, close to 50 % computational time is saved compared to the reference analysis. Having this in mind we conclude that even for a small problem like this where most of the nodes finally become enriched, an adaptive method can save considerable amount of computational effort.

6. Conclusions

In this paper we propose an adaptive enrichment methodology for the modelling of multiple and arbitrarily located delamination cracks in a laminated structure using an equivalent single-layer shell model. With this approach, the additional computational expense, associated with the complicated fracture process in laminated composites, can be limited while at the same time maintaining a high level of accuracy.

We can conclude that the adopted stress recovery method does improve the prediction of when to refine the model; however, not to a degree such that the enrichments can be initiated when the interlaminar stresses are close to the strength values. This should be viewed in light of the intended purpose of the stress recovery

Excerpt from ISBN 978-3-00-053387-7

method, which is only to improve the prediction of when to *refine* the model. Thus, we only need to be accurate enough such that this is done at approximately the right time and location.

Acknowledgements

The current work has been funded by the Swedish Strategic Vehicle Research and Innovation Programme on Vehicle and Traffic Safety via the project *Modelling crash behaviour in future lightweight composite vehicles - Step 1* which is gratefully acknowledged.

References

[1] ERTRAC. European Roadmap Safe Road Transport. Technical report, European Road Transport Research Advisory Council, 2011.

[2] J. Brouzoulis and M. Fagerström. An enriched shell element formulation for efficient modeling of multiple delamination propagation in laminates. *Compos. Struct.*, 126:196–206, feb 2015.

[3] J.J.C. Remmers, G.N. Wells, and R. de Borst. A solid-like shell element allowing for arbitrary delaminations. *Int. J. Numer. Meth. Eng.*, 58(13):2013–2040, 2003.

[4] N. Moës, J. Dolbow, and T. Belytschko. A finite element method for crack growth without remeshing. *Int. J. Numer. Meth. Eng.*, 46(1):131–150, 1999.

[5] A. Ahmed and L.J. Sluys. A computational model for the simulation of dynamic fracture in laminated composite plates. *J. Compos. Mater.*, 49(14):1717–1738, 2015.

[6] M. McElroy. An enriched shell element for delamination simulation in composite laminates. In *American Society for Composites 30th Technical Conference*, 2015.

[7] S. Hosseini, J.J.C Remmers, and C.V. Verhoosel. Propagation of delamination in composite materials with isogeometric continuum shell elements. *Int. J. Numer. Meth. Eng.*, 102:159–179, 2014.

[8] J.N. Reddy. *Mechanics of Laminated Composite Plates: Theory and Analysis*. Boca Raton, CRC Press, 1997.

[9] J. Främby, J. Brouzoulis, and M. Fagerström. Assessment of two methods for the accurate prediction of transverse stress distributions in laminates. *Compos. Struct.*, 140:602–611, apr 2016.

[10] E. Carrera. A priori vs. a posteriori evaluation of transverse stresses in multilayered orthotropic plates. *Compos. Struct.*, 48(4):245–260, 2000.

[11] A.K. Noor and M. Malik. An assessment of five modeling approaches for thermo-mechanical stress analysis of laminated composite panels. *Comput. Mech.*, 25:43–58, 2000.

[12] T. Kant and B.S. Manjunatha. On accurate estimation of transverse stresses in multilayer laminates. *Comput. Struct.*, 50(3):351–365, 1994.

[13] R. Rolfes and K. Rohwer. Improved transverse shear stresses in composite finite elements based on first order shear deformation theory. *Int. J. Numer. Meth. Eng.*, 40:51–60, 1997.

[14] O. Ochoa and J. Engblom. Analysis of progressive failure in composites. *Compos. Sci. Technol.*, 28(2):87–102, 1987.

[15] J. Främby, M. Fagerström and J. Brouzoulis. Adaptive modelling of delamination initiation and propagation using an equivalent single-layer shell approach. *Submitted*, 2016.

[16] N.E. Jansson and R. Larsson. A damage model for simulation of mixed-mode delamination growth. *Compos. Struct.*, 53(4):409–417, 2001.